Article

Chinese Science Bulletin

Geochemistry

November 2013 Vol.58 No.32: 3903–3913
doi: 10.1007/s11434-012-5607-z

A metasomatized mantle wedge origin for low-δ^{18}O olivine in late Cretaceous Junan and Qingdao basalts in the Sulu orogen

GUO Feng[1*], GUO JiangTao[1,2], WANG Yan[1], FAN WeiMing[1], LI ChaoWen[1], LI HongXia[1] & ZHAO Liang[1]

[1] *State Key Laboratory of Isotope Geochemistry, Guangzhou Institute of Geochemistry, Chinese Academy of Sciences, Guangzhou 510640, China;*
[2] *Graduate University of Chinese Academy of Sciences, Beijing 100049, China*

Received October 9, 2012; accepted November 16, 2012; published online June 20, 2013

The North China Block (NCB) experienced extensive lithospheric thinning and subsequent mantle accretion in the Mesozoic to Cenozoic, but their mechanism remains controversial. This paper reports *in situ* chemical and oxygen isotope analyses on olivine xenocrysts and porphyroclastic olivines in mantle xenoliths hosted in the late Cretaceous basalts from Junan and Qingdao, the Sulu orogen. The results show that all these olivines have low δ^{18}O values relative to normal mantle peridotite. The olivine xenocrysts and porphyroclastic olivines from Junan have Fo=87.5–89.8, δ^{18}O=4.1‰–5.2‰ with an average of 4.8‰; the porphyroclastic olivines from Qingdao also have Fo=89.0–89.9, δ^{18}O=4.1‰–5.2‰ with an average of 4.8‰. These peridotite xenoliths have petrological and geochemical affinities similar to newly accreted MORB-type mantle, we hence consider such low-δ^{18}O features in the olivines to inherit from a mantle wedge that was metasomatized by melts derived from the subducted oceanic crust, which had experienced high-temperature hydrothermal alteration to acquire the low-δ^{18}O signatures. Combined the existence of Cenozoic low-δ^{18}O basalts and garnet pyroxenite xenoliths (relicts of recycled oceanic crust) hosted in Cenozoic basalts in the NCB, the subducted oceanic crust likely played an important role in the lithospheric evolution of the NCB during the Mesozoic to Cenozoic.

metasomatized mantle wedge, subducted oceanic crust, low-δ^{18}O, olivine, late Cretaceous, North China Block

Citation: Guo F, Guo J T, Wang Y, et al. A metasomatized mantle wedge origin for low-δ^{18}O olivine in late Cretaceous Junan and Qingdao basalts in the Sulu orogen. Chin Sci Bull, 2013, 58: 3903–3913, doi: 10.1007/s11434-012-5607-z

The lithospheric thinning and subsequent mantle accretion of the North China Block (NCB) in the Mesozoic to Cenozoic is one of the hottest issue for international geologists. A large number of studies have shown that the NCB not only experienced extensive lithospheric thinning but also underwent mantle accretion since Mesozoic [1–8]. Evidence from mantle xenoliths entrained by Cenozoic basalts in the NCB indicated that the Cenozoic lithospheric mantle was composed mainly of chemically fertile but Sr-Nd isotopically depleted peridotites, analogues to depleted MORB-type mantle [1,3,5]. In recent years, such MORB-type mantle xenoliths were also found in late Cretaceous basalts from the Sulu orogen, suggesting that the mantle accretion might occur since the late Cretaceous [9–12]. Previous studies considered that the newly-accreted MORB-type mantle was formed through melting and thermal decay of the convective asthenosphere or melt-peridotite interaction in an extensional regime. Nevertheless, subduction of the Pacific oceanic slab beneath the Asian continent might also be a potential cause to modify the lithospheric mantle beneath the NCB since this subduction event occurred at least before the middle to late Cretaceous [13–15]. Also, geochemical studies on Cenozoic basalts in the eastern NCB indicate that the melting sources for these mafic lavas contained the component of the recycled Pacific oceanic crust [16–19]. However, there is no direct evidence for the presence of

*Corresponding author (email: guofengt@263.net)

slab-modified mantle peridotite in the NCB, which hampers to further understand the possible influence of such geodynamic processes on the evolution of the NCB lithospheric mantle.

The Earth is composed of several reservoirs with distinctive O isotopic compositions, so O isotope is widely applied to study the origin and evolution of magmas and to understand geodynamic processes such as mantle metasomatism by crustal materials during plate subduction [20–24]. It is generally accepted that normal mantle peridotites have a homogeneous O isotope composition, which is changed when crustal materials are recycled into the mantle through subduction and/or delamination processes. Whether the δ^{18}O of the modified mantle is decreased or elevated is mainly controlled by the O isotopic composition of recycled crustal materials. If the crustal component (e.g., pelagic sediments, low-T altered oceanic crust and carbonatites) has higher δ^{18}O values than that of normal mantle, the modified mantle is rich in ^{18}O, and vice versa. Up to now, few O isotope analyses have been performed for mantle xenoliths hosted by the Mesozoic to Cenozoic basalts, so it is unclear whether there exists O isotopic heterogeneity in the NCB lithospheric mantle.

Relative to traditional O isotope analytical techniques (e.g. O isotope analysis on mineral separates by the laser fluorination technique), the *in situ* O isotope analysis using a secondary ion mass spectrometer (SIMS) has overwhelming advantages in determining the O isotopic variation of single minerals or within a mineral. It can: (1) avoid the effect of the impure components within the mineral; (2) know whether there exists O isotopic heterogeneity between and within the analyzed minerals. If the mineral is O isotopically heterogeneous, the traditional analytical method cannot obtain the real O isotopic composition of the mineral but a mixture of mineral domains with different δ^{18}O values; and (3) effectively unravel the influence of exotic fluids or melts during mineral formation. Based on the above-mentioned advantages, in this paper we perform electron microprobe and *in situ* O isotope analyses on the olivine xenocrysts and porphyroclastic olivines in mantle xenoliths hosted by the late Cretaceous basalts from Junan and Qingdao in the Sulu orogen. The results show that all studied olivine crystals have relatively low δ^{18}O values with reference to the normal mantle, indicating an origin from a mantle wedge that was metasomatized by melts and/or fluids released from the subducted oceanic crust that had previously experienced high-T hydrothermal alteration.

1 Geological backgrounds and sample description

The Sulu orogen is the eastern extend of the Qinling-Dabie orogenic belt between the North China and South China Blocks (Figure 1(a)). Since the Triassic, the two blocks were united as a whole, and experienced a same tectonic regime during the Mesozoic to Cenozoic. The studying region is located in the interior of the Sulu orogen, of which Qingdao is located to the southeast of the Wulian-Yantai Fault and Junan is east to the giant Tan-Lu Fault.

Numerous previous studies have been carried out to reveal the regional tectonic evolution history. In summary, the basement rocks were composed mainly of low- to medium-grade metamorphic complexes of Mesoproterozoic to Neoproterozoic time termed as Fenzishan Group. During the end of Paleozoic to early Mesozoic, deep subduction of continental lithosphere resulted in the widespread ultrahigh-

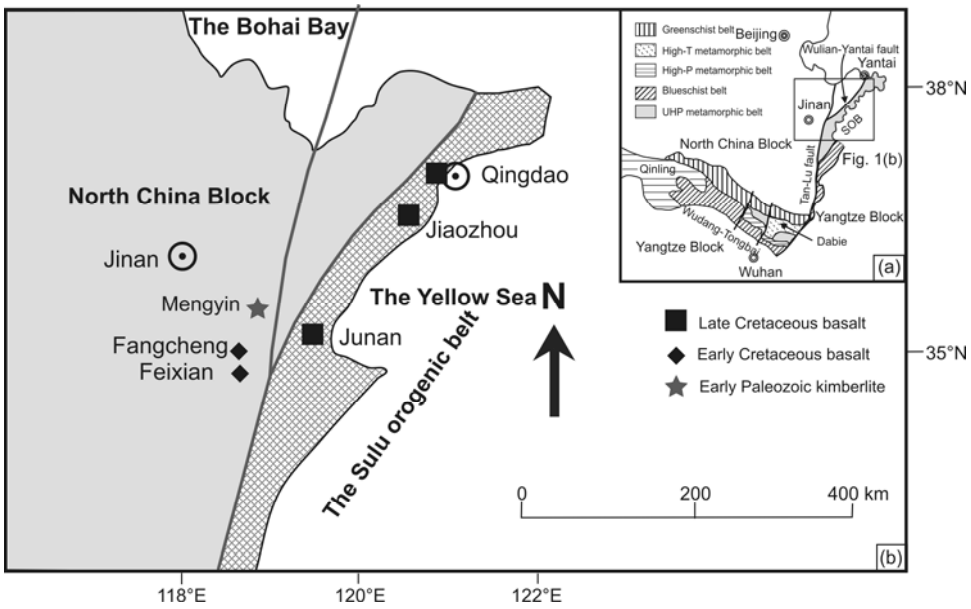

Figure 1 A simplified map showing the distribution of late Cretaceous basalts in the Sulu orogen, modified after [12]. SO: The Sulu orogen.

pressure (UHP) metamorphism and subsequent exhumation of the UHP rocks [25,26]. During the late Mesozoic, the region was under an extensional regime, leading to emplacement of voluminous mantle-derived and crust-derived magmas and the resultant mineralization, as well as extensive eruption of volcanic lavas as the Qingshan Formation [27–29]. The Middle to Upper Cretaceous comprises a set of sandy conglomerates termed as the Wansgshi Formation with similar affinities to foreland basin, with sporadic distribution of basalts (Figure 1(b)). From the east to west, the mafic lavas include the basaltic dikes at Pishikou of Qingdao (~82 Ma) [11], olivine basalts at Daxizhuang of Jiaozhou (~74 Ma) [9] and basaltic agglomerates at Junan (~67 Ma) [10].

These late Cretaceous basalts generally show geochemical features similar to the oceanic island basalts (OIBs), e.g. low SiO_2, high MgO and alkali, positive Nb-Ta anomalies and Pb depletion in primitive mantle-normalized spidergrams and low radiogenic Sr and moderately radiogenic Nd compositions [9–11], except for the relatively radiogenic Sr ($^{87}Sr/^{86}Sr_i$>0.7045) for the Qingdao basaltic dikes [11]. Such geochemical features are also common for the Cenozoic basalts in eastern China [16–18].

The studied olivines were collected from the basaltic dikes in Qingdao and basaltic agglomerates in Junan. The basalts are dark to dark grey, and are porphyric with predominant clinopyroxene phenocrysts with rare olivine and plagioclase. The matrix is mainly composed of clinopyroxene, olivine and plagioclase microcrystallines and glasses. In the basaltic agglomerates in Junan, there also exist olivine and clinopyroxene xenocrysts. The xenocrystic olivines show clear contact boundary with the host basalts (Figure 2(a) and (b)). The olivines in mantle xenoliths show porphyroclastic to equigranular texture. The mantle xenoliths are spinel lherzolites and low-T alteration can also be observed between olivine crystals (Figure 2(c) and (d)).

2 Analytical techniques

Back-scattered electron (BSE) images and chemical compositions of minerals were performed on a JEO LIXA-8100 Electron Microprobe at the Guangzhou Institute of Geochemistry (GIG), Chinese Academy of Sciences (CAS). Normal operating conditions were 15 kV accelerating voltage, 10 nA beam current, and 2 μm beam diameter. Extended counting time was used following the method described in Sobolev et al. [30]. Based on repeated analyses of the natural and synthetic standards, relative analytical uncertainty is <2% for the major elements and <5% for minor elements. The analytical results of olivine are listed in Table 1.

The *in situ* olivine oxygen isotope analysis was performed on the Cameca IMS-1280 at the Institute of Geology and Geophysics, CAS. The O isotope results are reported in the conventional $\delta^{18}O$ notation relative to the reference standard VSMOW. Detailed description of the analytical procedure was reported in [31]. San Carlos olivine standard grains were mounted adjacent to the thick-polished sections in epoxy. The Cs^+ primary beam was accelerated at 10 kV with an intensity of ca. 2 nA. The spot size was about 20 μm in diameter (10 μm beam diameter +10 μm raster). An electron gun was used to compensate for sample charging during analysis. Secondary ions were extracted with a −10 kV potential. Oxygen isotopes (^{18}O and ^{16}O) were measured in a multi-collector mode with two off-axis Faraday cups with each analysis consisting of 20 cycles ×4 counting time. External reproducibility of olivine standards was typically better than 0.4% (2 SD) for $\delta^{18}O$. During the analysis, the San Carlos olivine standard yields $\delta^{18}O$=5.27±0.08‰ (2σ, n=32), similar to the recommended $\delta^{18}O$ value of 5.35‰ within the analytical errors [32]. The O isotopic analytical results of the studied olivine crystals and the San Carlos olivine standard are listed in Table 2.

3 Results

3.1 Olivine xenocrysts in Junan basalts

The olivine xenocrysts are euhedral to subhedral in shape (Figure 2(a) and (b)) and span a SiO_2 range of 39.1% to 40.7%, a MgO range of 45.3% to 47.3%, a NiO range of 0.31% to 0.37%, and a MnO range of 0.13% to 0.19% with CaO <0.1%. These olivines are relatively homogeneous with a forsterite (Fo) content varying between 88.7 and 89.5, similar to those of chemically fertile mantle peridotites [33]. They yield a $\delta^{18}O$ range of 4.1‰ to 5.3‰ with an average of 4.7‰, obviously lower $\delta^{18}O$ than those in normal mantle peridotites ($\delta^{18}O$=5.1‰–5.4‰) [34].

3.2 Olivine of mantle xenoliths in Junan basalts

The olivines in mantle xenoliths show porphyroclastic to equigranular texture (Figure 2(c) and (d)) and span a SiO_2 range of 40.5% to 43.1%, a MgO range of 43.7% to 48.3%, a NiO range of 0.33% to 0.39%, and a MnO range of 0.12% to 0.17% with CaO <0.1%. These olivines are also relatively homogeneous with a Fo range varying between 87.5 and 88.4, a little lower Fo than those of chemically fertile mantle peridotites [33]. They yield a $\delta^{18}O$ range of 4.5‰ to 5.3‰ with an average of 5.0‰, slightly lower $\delta^{18}O$ than those in normal mantle peridotites [34].

3.3 Olivine of mantle xenoliths in Qingdao basalts

The olivines are also porphyroclastic to equigranular (Figure 2(e) and (f)) and span a SiO_2 range of 40.0% to 41.6%, a MgO range of 47.3% to 50.5%, a NiO range of 0.34% to 0.38%, and a MnO range of 0.12% to 0.17% with CaO <0.1%. These olivines are also relatively homogeneous with

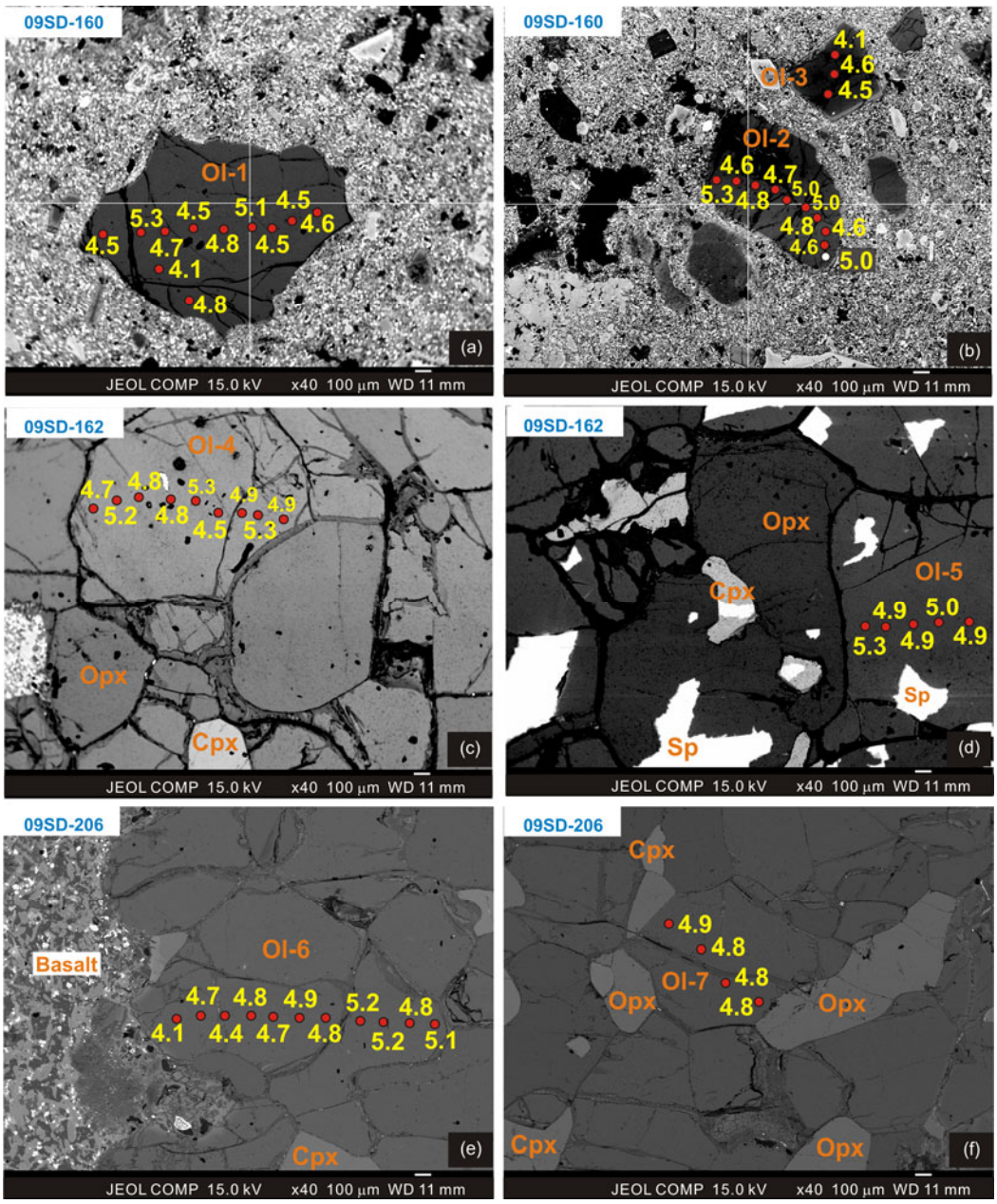

Figure 2 The *in situ* O isotopic compositions of olivine xenocrysts and olivine crystals in mantle xenoliths hosted in late Cretaceous Junan and Qingdao basalt. The numbers of olivine such as Ol-1 to 7 are corresponding to those listed in Tables 1 and 2. (a) and (b) showing the results of the xenocrystic olivines from the Junan basalts; (c) and (d) showing the results of mantle xenoliths from the Junan basalts; (e) and (f) showing the results of mantle xenoliths from the Qingdao basalts. Ol, Olivine; Cpx, clinopyroxene; Opx, orthopyroxene; Sp, spinel.

a Fo range of 89.0–89.9, similar to the low-MgO peridotite xenoliths reported by Zhang et al. [12] and other lherzolite xenoliths hosted in Cenozoic basalts in eastern China. They yield a δ^{18}O range of 4.2‰ to 5.3‰ with an average of 4.9‰, lower δ^{18}O than those in normal mantle peridotites [34].

4 Discussion

The analyzed olivines from the Junan and Qingdao are chemically fertile and low δ^{18}O relative to normal mantle peridotites (Figure 3(a)). At one hand, both analyzed olivines and the San Carlos olivine standards (Fo=90) have quite similar chemical compositions, so the effect of mass fractionation on O isotopic variation during SIMS analysis can be negligible. At the other hand, surface low-T alteration can lead to increase of δ^{18}O in the altered parts of the mineral (Figure 3(b)), we hence consider that the lower δ^{18}O values in the studied olivines than those of normal mantle do reflect their primary low-δ^{18}O signatures.

To summarize the O isotopic variations, the analyzed olivines do not show any linear relationship between the

Table 1 Representative chemical compositions of olivine xenocrysts and porphyroclastic olivines in mantle xenoliths hosted in late Cretaceous Junan and Qingdao basalts from the Sulu orogen[a)]

Sample	No. of olivine	SiO_2	NiO	CaO	Al_2O_3	FeO	MgO	MnO	Cr_2O_3	Total	Fo
		Olivine xenocrysts in Junan basalts									
09SD-160	Ol-1	40.34	0.31	0.06	0.05	9.80	46.72	0.15	0.02	97.45	89.5
	Ol-1	40.42	0.34	0.06	0.03	10.03	46.64	0.19	0.02	97.73	89.2
	Ol-1	40.21	0.33	0.07	0.02	10.09	46.54	0.16	–	97.42	89.2
	Ol-1	40.22	0.35	0.04	0.01	10.16	47.13	0.15	0.01	98.06	89.2
	Ol-1	40.70	0.32	0.04	0.02	10.15	47.34	0.14	0.00	98.70	89.3
	Ol-1	40.51	0.36	0.04	0.01	10.25	47.08	0.16	–	98.41	89.1
	Ol-1	39.94	0.35	0.04	0.01	10.21	46.23	0.16	0.01	96.94	89.0
	Ol-1	40.26	0.37	0.04	0.02	10.06	46.53	0.14	0.02	97.43	89.2
	Ol-1	39.10	0.35	0.04	0.02	10.29	45.34	0.16	0.01	95.31	88.7
	Ol-1	40.20	0.34	0.04	0.01	10.20	46.70	0.15	0.01	97.66	89.1
	Ol-1	40.30	0.36	0.05	0.02	10.25	46.76	0.15	0.00	97.87	89.1
	Ol-2	40.17	0.34	0.07	0.02	10.47	46.72	0.17	0.00	97.95	88.8
	Ol-2	40.07	0.33	0.06	0.03	10.32	46.54	0.16	0.02	97.51	88.9
	Ol-2	40.13	0.32	0.06	0.02	10.35	46.17	0.16	0.03	97.23	88.8
	Ol-2	40.19	0.32	0.07	0.10	10.32	46.51	0.13	0.01	97.65	88.9
	Ol-2	40.01	0.33	0.06	0.02	10.39	46.57	0.18	0.01	97.57	88.9
	Ol-3	39.81	0.33	0.07	0.03	10.32	46.54	0.16	0.01	97.26	88.9
	Ol-3	39.95	0.32	0.06	0.02	10.31	46.54	0.17	0.01	97.37	89.0
	Ol-3	39.94	0.33	0.07	0.02	10.26	46.54	0.13	–	97.28	89.0
	Ol-3	40.02	0.31	0.07	0.02	10.37	46.40	0.14	0.02	97.34	88.9
	Ol-3	39.64	0.35	0.08	0.03	10.26	46.96	0.14	0.02	97.47	89.1
		Olivines in mantle xenoliths hosted in Junan basalts									
09SD-162	Ol-4	41.60	0.35	0.08	0.06	11.36	44.49	0.16	0.02	98.12	87.5
	Ol-4	41.37	0.35	0.06	0.03	11.35	45.35	0.16	0.03	98.69	87.7
	Ol-4	41.62	0.36	0.08	0.02	11.03	45.52	0.17	0.00	98.79	88.0
	Ol-4	41.59	0.34	0.06	0.03	11.19	46.12	0.15	0.02	99.50	88.0
	Ol-4	42.02	0.36	0.08	0.04	11.02	45.45	0.15	0.04	99.15	88.0
	Ol-4	41.85	0.35	0.07	0.03	11.29	44.45	0.14	0.02	98.20	87.5
	Ol-4	41.30	0.37	0.06	0.03	11.32	46.25	0.14	0.02	99.50	87.9
	Ol-4	43.13	0.34	0.07	0.03	10.93	43.70	0.15	0.02	98.36	87.7
	Ol-4	41.12	0.35	0.07	0.04	11.26	44.85	0.17	0.02	97.88	87.7
	Ol-4	41.87	0.38	0.05	0.02	11.04	46.57	0.15	0.00	100.08	88.3
	Ol-4	40.47	0.37	0.07	0.04	11.22	46.43	0.16	0.01	98.76	88.1
	Ol-4	42.18	0.35	0.06	0.02	11.42	45.71	0.17	0.03	99.92	87.7
	Ol-4	41.87	0.35	0.06	0.05	11.28	47.10	0.15	0.03	100.90	88.2
	Ol-4	42.56	0.34	0.07	0.05	11.35	44.74	0.15	0.03	99.29	87.5
	Ol-4	41.85	0.33	0.10	0.09	11.12	45.41	0.15	0.03	99.08	87.9
	Ol-4	41.60	0.34	0.08	0.12	11.23	44.64	0.17	0.05	98.23	87.6
	Ol-4	41.30	0.34	0.08	0.04	11.30	48.27	0.12	0.03	101.47	88.4
	Ol-5	41.97	0.36	0.05	0.02	11.24	45.78	0.14	0.03	99.59	87.9
	Ol-5	41.85	0.36	0.06	0.05	11.13	45.66	0.14	0.03	99.29	88.0
	Ol-5	41.74	0.36	0.08	0.05	11.19	45.51	0.14	0.03	99.09	87.9
	Ol-5	41.78	0.35	0.06	0.04	11.11	47.01	0.16	0.01	100.52	88.3
	Ol-5	42.00	0.36	0.05	0.03	11.29	45.23	0.15	0.01	99.12	87.7
	Ol-5	42.23	0.34	0.08	0.06	11.09	47.17	0.14	0.02	101.13	88.4
	Ol-5	41.09	0.35	0.08	0.06	11.42	46.34	0.17	0.02	99.52	87.9
	Ol-5	41.76	0.35	0.06	0.04	11.06	45.13	0.14	0.01	98.56	87.9
	Ol-5	41.91	0.33	0.11	0.17	11.41	46.89	0.15	0.04	101.02	88.0
	Ol-5	42.22	0.35	0.07	0.05	11.30	45.44	0.15	0.00	99.58	87.8
	Ol-5	41.49	0.35	0.06	0.03	11.38	45.80	0.15	0.03	99.28	87.8
	Ol-5	40.78	0.36	0.06	0.03	11.38	47.03	0.13	0.02	99.79	88.1
	Ol-5	41.43	0.36	0.07	0.04	11.30	44.90	0.15	0.03	98.28	87.6

(*To be continued on the next page*)

(*Continued*)

Sample	No. of olivine	SiO_2	NiO	CaO	Al_2O_3	FeO	MgO	MnO	Cr_2O_3	Total	Fo
		Olivines of mantle xenoliths hosted in Qingdao basalts									
09SD-206	Ol-6	40.02	0.36	0.10	0.03	10.12	50.46	0.16	0.03	101.27	89.9
	Ol-6	40.21	0.34	0.09	0.04	10.20	47.55	0.16	0.02	98.61	89.3
	Ol-6	40.49	0.34	0.10	0.04	10.37	47.30	0.14	0.02	98.79	89.0
	Ol-6	40.49	0.36	0.10	0.03	10.34	48.98	0.15	0.02	100.47	89.4
	Ol-6	40.54	0.35	0.10	0.03	10.34	47.25	0.17	0.02	98.79	89.1
	Ol-6	40.58	0.36	0.09	0.03	10.32	47.93	0.12	0.02	99.45	89.2
	Ol-6	40.62	0.34	0.09	0.03	9.92	47.73	0.16	0.01	98.90	89.6
	Ol-6	40.71	0.34	0.09	0.03	10.33	47.54	0.13	0.02	99.19	89.1
	Ol-6	40.73	0.34	0.09	0.03	10.45	47.99	0.17	0.03	99.82	89.1
	Ol-6	40.79	0.35	0.09	0.03	10.41	48.12	0.15	0.02	99.96	89.2
	Ol-6	40.80	0.36	0.09	0.06	10.46	48.09	0.13	0.09	100.09	89.1
	Ol-6	40.88	0.34	0.09	0.03	10.51	47.97	0.17	0.01	100.00	89.1
	Ol-6	40.90	0.38	0.09	0.03	10.57	48.50	0.15	0.03	100.64	89.1
	Ol-6	40.95	0.34	0.09	0.02	10.24	47.62	0.14	0.03	99.44	89.2
	Ol-6	40.99	0.36	0.09	0.02	10.33	47.95	0.16	0.01	99.90	89.2
	Ol-7	41.13	0.37	0.09	0.03	10.34	48.51	0.15	0.01	100.62	89.3
	Ol-7	41.16	0.36	0.08	0.03	10.36	48.24	0.13	0.01	100.37	89.2
	Ol-7	41.17	0.36	0.09	0.02	10.36	48.68	0.14	0.04	100.85	89.3
	Ol-7	41.18	0.36	0.08	0.03	10.45	48.57	0.15	0.01	100.81	89.2
	Ol-7	41.21	0.35	0.10	0.04	10.34	47.37	0.14	0.02	99.57	89.1
	Ol-7	41.23	0.34	0.08	0.03	10.45	47.76	0.15	0.03	100.06	89.1
	Ol-7	41.34	0.36	0.09	0.03	10.29	48.28	0.13	0.02	100.55	89.3
	Ol-7	41.40	0.36	0.09	0.03	10.31	48.08	0.16	0.02	100.44	89.3
	Ol-7	41.57	0.35	0.09	0.02	10.44	48.27	0.16	0.02	100.92	89.2

a) "–" denotes the value lower than the detection limit of the electron microprobe. The analytical technique is described in [30]. During analysis, the counting time for Si, Mg, Fe, Ca, Al is 90 s, 120 s for Mn and Cr and 150 s for Ni, respectively. The analytical spots are listed from rim to core and then rim. The numbers of olivine are corresponding to those listed in Figure 2.

distance from rim and the $\delta^{18}O$, e.g. from the contact boundary between host basalt and olivine to the core portion, the $\delta^{18}O$ show random variations against the distance (Figure 3(a)). The analyzed low-$\delta^{18}O$ olivines are similar to those in UHP garnet peridotites ($\delta^{18}O$=3.6‰–5.3‰) [35,36] and also to some olivine phenocrysts in Cenozoic basalts from the Sulu orogen [16,18], but clearly distinctive from the olivines in Mesozoic basalts and their hosting pyroxenite xenoliths (Figure 4(a)) [37]. In the following, we will first understand the origin of the low-$\delta^{18}O$ olivines and then discuss the possible implications for the Mesozoic to Cenozoic lithospheric evolution beneath the NCB.

4.1 Origin of low-$\delta^{18}O$ olivine

Low-$\delta^{18}O$ magmas are generally considered to form in continental rifts or spreading oceanic ridges [24]. In a continental rift, the low-$\delta^{18}O$ meteoric water can be effectively recycled to the melting source along the fault or crack, melts derived from such a mixed source will naturally have low $\delta^{18}O$. In the oceanic lithosphere, high-T fluid-rock interaction or metamorphism occurs at the lower oceanic gabbroic crust or mantle peridotite to forms the low-$\delta^{18}O$ feature, whereas the upper basaltic crust experiences low-T alteration to form high-$\delta^{18}O$ altered crust [40,41].

Up to now, whether there exists O isotopic heterogeneity in the mantle reservoir is still of great debate. Harmon and Hoefs [42] believed that there might exist several mantle reservoirs with distinctive $\delta^{18}O$ because the olivine phenocrysts in basalts from different tectonic settings show systematic O isotopic variation. Based on the O isotopic difference of olivine among several types of OIBs, Eiler et al. [43] also proposed that the $\delta^{18}O$ of mantle reservoirs were heterogeneous. Gurenko et al. [44] noted that the $\delta^{18}O$ variation in olivines from the Canary Islands basalts was attributed to source heterogeneous, e.g. the melts derived from the peridotites have relatively low $\delta^{18}O$ (5.2‰), whereas the magmas derived from metasomatized pyroxenites have higher $\delta^{18}O$ (5.9‰). Nevertheless, *in situ* O isotope analyses on olivine from the low-$\delta^{18}O$ OIBs from both the Iceland and Hawaii regions suggested that the low-$\delta^{18}O$ features were formed by assimilation of low-$\delta^{18}O$ oceanic crust [32,45,46]. The olivine phenocrysts in basalts from the Kamchatka arc have higher $\delta^{18}O$ than normal mantle, which

Table 2 *In situ* O isotopic compositions of the analyzed olivine crystals hosted in the late Cretaceous Junan and Qingdao basalts and San Carlos standard[a)]

Olivine xenocrysts from Junan			Mantle xenoliths from Junan			Mantle xenoliths from Qingdao			San Carlos standard	
No. of olivine	Distance to rim (μm)	$\delta^{18}O\pm2\sigma$ (‰)	No. of olivine	Distance to rim (μm)	$\delta^{18}O\pm2\sigma$ (‰)	No. of olivine	Distance to rim (μm)	$\delta^{18}O\pm2\sigma$ (‰)	No. of olivine	$\delta^{18}O\pm2\sigma$ (‰)
Ol-1	150	4.55±0.38	Ol-4	1100	4.91±0.28	Ol-6	50	5.14±0.22	sancarlos@1	5.10±0.28
Ol-1	300	4.47±0.24	Ol-4	880	5.33±0.30	Ol-6	180	4.83±0.31	sancarlos@2	5.45±0.23
Ol-1	400	4.47±0.25	Ol-4	800	4.91±0.24	Ol-6	300	5.23±0.34	sancarlos@3	5.14±0.32
Ol-1	520	5.09±0.18	Ol-4	700	4.50±0.22	Ol-6	450	5.17±0.38	sancarlos@4	5.29±0.37
Ol-1	680	4.77±0.27	Ol-4	600	5.26±0.21	Ol-6	580	4.77±0.14	sancarlos@5	5.43±0.26
Ol-1	1300	5.28±0.24	Ol-4	520	4.82±0.26	Ol-6	730	4.89±0.39	sancarlos@6	5.05±0.29
Ol-1	900	4.51±0.30	Ol-4	340	4.82±0.29	Ol-6	900	4.68+0.26	sancarlos@7	5.37±0.24
Ol-1	110	4.74±0.34	Ol-4	180	5.18±0.36	Ol-6	1100	4.75+0.36	sancarlos@8	5.20±0.18
Ol-1	1500	4.54±0.24	Ol-4	90	4.66±0.32	Ol-6	1250	4.39±0.34	sancarlos@9	5.12±0.25
Ol-1	1200	4.09±0.37	Ol-5	100	5.27±0.26	Ol-6	1400	4.70±0.31	sancarlos@10	5.35±0.40
Ol-1	1000	4.77±0.26	Ol-5	200	4.92±0.30	Ol-6	1550	4.15±0.38	sancarlos@11	5.36±0.31
Ol-2	50	5.30±0.33	Ol-5	350	4.95±0.24	Ol-7	100	4.90±0.36	sancarlos@12	5.36±0.20
Ol-2	120	4.61±0.30	Ol-5	540	4.96±0.32	Ol-7	350	4.78±0.19	sancarlos@13	5.30±0.29
Ol-2	240	4.76±0.30	Ol-5	700	4.93±0.26	Ol-7	600	4.83±0.17	sancarlos@14	5.41±0.21
Ol-2	350	4.65±0.27				Ol-7	750	4.84±0.26	sancarlos@15	5.32±0.22
Ol-2	480	4.97±0.29							sancarlos@16	5.00±0.29
Ol-2	550	4.99±0.34							sancarlos@17	5.35±0.36
Ol-2	670	4.77±0.21							sancarlos@18	5.26±0.36
Ol-2	800	4.59±0.30							sancarlos@19	5.35±0.33
Ol-2	900	4.58±0.27							sancarlos@20	5.61±0.30
Ol-2	1000	4.97±0.34							sancarlos@21	5.38±0.15
Ol-3	450	4.64±0.36							sancarlos@22	5.15±0.15
Ol-3	300	4.10±0.23							sancarlos@23	5.23±0.28
Ol-3	150	4.53±0.35							sancarlos@24	5.12±0.27
									sancarlos@25	5.05±0.26
									sancarlos@26	5.24±0.30
									sancarlos@27	5.15±0.27
									sancarlos@28	5.08±0.35
									sancarlos@29	5.40±0.20
									sancarlos@30	5.02±0.33
									sancarlos@31	5.49±0.30
									sancarlos@32	5.24±0.19

a) The San Carlos olivine standard yields $\delta^{18}O = 5.27\pm0.08‰$ (n=32), consistent with the recommended $\delta^{18}O$ value [32].

were considered to form through mixing of magmas derived from different mantle sources and/or disequilibrium diffusion-driven O isotope fractionation [47], with the high-$\delta^{18}O$ magma component from a mantle wedge strongly modified by ^{18}O-rich fluids. Therefore, recycling of crustal component through subduction is a potential mechanism to form the O isotopic heterogeneity in the mantle source [24].

According to the previous studies [9,10,12], the studied mantle xenoliths are chemically fertile, equilibrant to the low-MgO lherzolites. However, the host Junan basalts have Mg# between 66–71 (our unpublished data), their crystallizing olivine should have a Fo range of 70–80, much lower than the olivine xenocrysts (Fo ~89) and porphyroclastic olivine in mantle xenoliths (Fo=87.5–89.9). Also, the studied olivine xenocrysts and porphyroclastic olivines are slightly lower Fo than those olivines (Fo>90 and up to 92) in normal oceanic mantle peridotites. Consequently, both the olivine xenocrysts and porphyroclastic olivines were neither crystallizing phases from the host basalts nor the residual minerals after extensive basalt extraction of normal mantle peridotites. A likely explanation is that these olivines were formed either through melt-peridotite interaction in a subduction

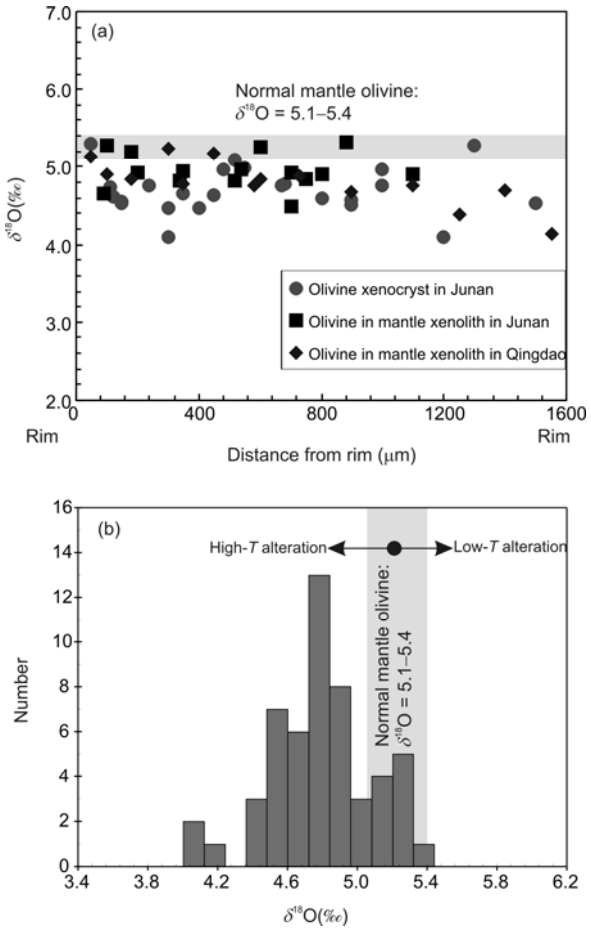

Figure 3 The statistic δ^{18}O values of olivine (a) and the relationship between δ^{18}O of olivine and the distance from the mineral rim. The δ^{18}O value of olivine in normal mantle is referred to [34]. In (b), the influence of alteration types on the δ^{18}O values of olivine are referred to [40,41].

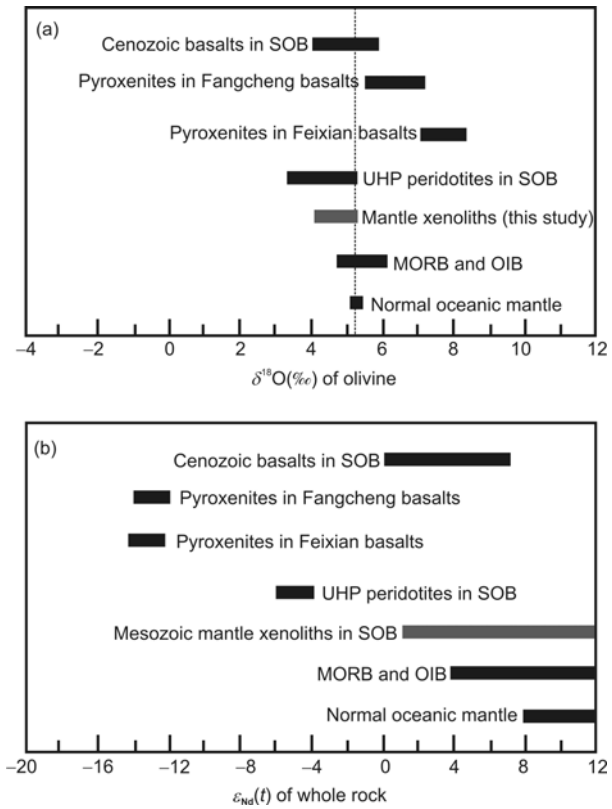

Figure 4 Comparison of δ^{18}O of olivine (a) and $\varepsilon_{Nd}(t)$ of whole rock (b) among the mafic rocks in different era. Data sources: Oceanic mantle peridotite [34], MORB and OIB [42,43]; UHP garnet peridotites in the Sulu orogen [35,36]; Cenozoic basalts in the Sulu orogen [16,18]; pyroxenites in the Mesozoic Feixian picrites [37]; mantle xenoliths in late Cretaceous basalts from the Sulu orogen (this study); Nd isotope data [12]; pyroxenites in the Mesozoic Fangcheng basalts [48 and our unpublished data].

channel or as residual phases of olivine pyroxenites after melting [24].

In the case of melt-peridotite interaction, the melt reacts with the surface of the olivine, so the reacted olivine will exhibit chemical and O isotopic variations in the rim while its interior preserves the near-primary features. Thus the systematic compositional and δ^{18}O zoning will be observed in the reacted olivine, in contrast with the analyzed olivines that show random variation in δ^{18}O (Figures 2 and 3(a)). This suggests that the δ^{18}O variation in the studied olivine was unlikely to be formed through interaction between the host basalts and the xenoliths. However, if the melt-peridotite interaction occurs to form low-δ^{18}O pyroxenites in the subduction channel, melting of the reacted pyroxenites will leave residual peridotites with homogeneous chemical and O isotopic compositions in the olivine. At mantle conditions, the O isotopic fingerprints caused by melt-peridotite interaction can hardly be preserved at the base of lithosphere, since the convective asthenosphere has high temperature and mantle convection will homogenize the O isotopic variation due to rapid O isotope diffusion. For this reason, these low-δ^{18}O pyroxenites should be stayed above the boundary between the lithosphere-asthenosphere so that the low-δ^{18}O signature in olivine can still be preserved.

Although the garnet peridotites in the Sulu orogen also have similar low-δ^{18}O features [35,36], their relatively evolved Sr-Nd isotopic compositions ($\varepsilon_{Nd}(t)$=−5.8 to −3.6, $^{87}Sr/^{86}Sr_i$=0.7086 to 0.7096) are quite different from the studied mantle xenoliths (Figure 4(b)). We therefore conclude that the mantle xenoliths hosted by the Qingdao and Junan basalts were unlikely to be derived from the deeply subducted lithospheric mantle of the South China Block. Similarly, the O and Nd isotopic differences (Figure 4) between the studied samples and the olivine pyroxenite xenoliths hosted in early Cretaceous basalts in the adjacent Fangcheng and Feixian area argue against an origin of the enriched lithospheric mantle extensively modified by melts or fluids derived from the Triassic deeply subducted continental crust [37,48].

As discussed above, the studied mantle xenoliths show petrologic and geochemical similarities to those spinel lherzolites hosted in Cenozoic basalts in eastern China [2–8], e.g. relatively low Fo, N-MORB-like REE patterns of cli-

nopyroxenes and MORB-type Sr-Nd isotopic signatures [9,10,12]. Although there lack relative reports about the O isotopic compositions of olivine from the mantle peridotites in the NCB, it is predicted that the newly accreted mantle transformed from the asthenosphere through mantle melting should have similar O isotopic compositions to normal mantle peridotites [17,28,34], different from the low-δ^{18}O features observed in this study. Therefore, we consider that these mantle xenoliths and xenocrystic olivines represent the newly accreted mantle which had been modified by low-δ^{18}O crust-derived melt.

Previous studies on the ophiolites suites revealed that alteration of the oceanic lithosphere could form two distinctive trends in terms of O isotopes: (1) the upper oceanic crust experienced low-T seawater alteration and became rich in ^{18}O; and (2) the lower gabbroic crust and upper peridotitic mantle underwent high-T hydrothermal alteration or metamorphism and became poor in ^{18}O [40,41]. In the course of oceanic slab subduction, there also exist such two distinctive mantle wedges [24]: (1) an ^{18}O-rich mantle wedge that is predominantly modified by fluids or melts released from the subducted oceanic upper crust and its overlying pelagic sediments; and (2) the other ^{18}O-poor mantle wedge that is predominantly modified by fluids or melts derived from the high-T altered lower gabbroic crust or upper peridotitic mantle. The relatively low Fo and low-δ^{18}O features of the studied olivines likely represent the mantle wedge metasomatized by melts from the high-T altered lower gabbroic oceanic crust.

4.2 Implications for lithospheric evolution beneath the NCB

In recent years, the Cenozoic low-δ^{18}O basalts in the Sulu orogen have been discovered and were originally related to the involvement of subducted oceanic lithosphere [16,18]. Yu et al. [49] reported low-δ^{18}O garnet pyroxenite xenoliths hosted in Cenozoic basalts in the northeastern NCB and considered them to represent the relicts of the subducted oceanic crust that had experienced high-T alteration or metamorphism. Zheng [24] considered that the low-δ^{18}O peridotites and pyroxenites in the overlying mantle wedge would have formed through metasomatism by low-δ^{18}O melts derived from subducting oceanic crust during slab-mantle interaction in oceanic subduction channels.

Evidence from the motion trait of the Pacific Oceanic plate showed that the NE Asian continental margin had interacted with the Pacific slab at least since late Mesozoic [13,14]. In both the Junan and Qingdao regions, there also exist high-MgO peridotite xenoliths that represented the old and refractory lithospheric mantle beneath the NCB [10,12]. To summarize the above discussion, we envisage a petrogenetic model to interpret the origin of the low-δ^{18}O olivines in the Sulu orogen.

(1) The subducted Pacific oceanic crust experienced high-T alteration to obtain the low-δ^{18}O signatures [16–18,49]. (2) These low-δ^{18}O metagabbro was partially melted to generate low-δ^{18}O felsic melts, which reacted with the overlying mantle peridotites to form the low-δ^{18}O mantle sources [16–18]. (3) Melting of the metasomatized mantle wedge occurred, of which the low-δ^{18}O source (including metasomatized peridotites [16–18] and garnet pyroxenites [49]) was melted to produce the low-δ^{18}O basalts, such as the Cenozoic basalts in the Sulu orogen. These low-δ^{18}O mantle relicts, together with the overlying old lithospheric mantle–represented by high-MgO peridotite xenoliths, were brought to the surface by the host basalts [9,10,12]. The parental rocks for the low-δ^{18}O olivines were probably the metasomatized olivine pyroxenites, which were melted to form the low-δ^{18}O continental basalts in the Sulu orogen and even throughout the NCB [16,18], leaving the low-δ^{18}O relict peridotites [24]. If our conclusions are reasonable, subduction of the Pacific oceanic slab and the resulted replacement of the newly accreted mantle wedge to the old and refractory lithospheric mantle beneath the NCB might be an important mechanism for the lithospheric thinning and the subsequent mantle accretion [16].

5 Concluding remarks

The new chemical and *in situ* O isotopic analyses on olivine xenocrysts and olivines in mantle xenoliths hosted by the late Cretaceous basalts from Junan and Qingdao, the Sulu orogen, provide important constraints on the evolution of the lithospheric mantle beneath the NCB. These olivines have low Fo and δ^{18}O values relative to normal mantle though their parental rocks have similar petrological, elemental and Sr-Nd isotopic features to the MORB-type mantle. They are likely derived from a mantle wedge that was metasomatized by melts derived from the high-T altered lower oceanic crust. Combined the existence of Cenozoic low-δ^{18}O basalts and low-δ^{18}O garnet pyroxenite xenoliths (relicts of recycled oceanic crust) hosted in the Cenozoic basalts in the NCB, the subducted Pacific oceanic crust might play an important role in the evolution of the lithospheric mantle during the Mesozoic to Cenozoic. The westward subduction of the Pacific Ocean would have not only caused the lithospheric thinning and mantle replacement, but also transformed the mantle wedge metasomatized by low-δ^{18}O melts or fluids into the newly accreted mantle. These metasomatized mantle wedge materials were likely an important source for the late Cretaceous to Cenozoic basalts in eastern China and also for the newly accreted mantle.

We are grateful for Prof. X. H. Li, Dr. Q. L. Li and G. Q. Tang for their help in the SIMS O isotope analysis and for L. L. Chen for her help in electron microprobe analysis. Thanks are also due to Prof. Y. F. Zheng and two anonymous referees for their critical reviews and comments, which

help improve the manuscript. This work was supported by the National Natural Science Foundation of China (90914009 and 41121002).

1 Menzies M A, Fan W M, Zhang M. Palaeozoic and Cenozoic lithoprobes and the loss of >120 km of Archaean lithosphere, Sino-Korean craton, China. In: Prichard H M, Alabaster T, Harris N B W, et al, eds. Magmatic Processes and Plate Tectonics. Geol Soc Spec Pub, 1993, 76: 71–81

2 Fan W M, Zhang H F, Baker J, et al. On and off the North China Craton: Where is the Archaean keel? J Petrol, 2000, 41: 933–950

3 Zheng J P, O'Reilly S Y, Griffin W, et al. Relict refractory mantle beneath the eastern North China block: Significance for lithosphere evolution. Lithos, 2001, 57: 43–66

4 Zheng J P, Griffin W L, O'Reilly S Y, et al. Mechanism and timing of lithospheric modification and replacement beneath the eastern North China Craton: Peridotitic xenoliths from the 100 Ma Fuxin basalts and a regional synthesis: Geochim Cosmochim Acta, 2007, 71: 5203–5225

5 Xu Y G. Thermo-tectonic destruction of the Archaean lithospheric keel beneath the Sino-Korean Craton in China: Evidence, Timing and Mechanism. Phys Chem Earth (A), 2001, 26: 747–757

6 Xu Y G, Blusztajn J, Ma J L, et al. Late Archean to Early Proterozoic lithospheric mantle beneath the western North China craton: Sr-Nd-Os isotopes of peridotite xenoliths from Yangyuan and Fansi. Lithos, 2008, 102: 25–42

7 Gao S, Rudnick R, Carlson, R W, et al. Re-Os evidence for replacement of ancient mantle lithosphere beneath the North China Craton. Earth Planet Sci Lett, 2002, 198: 307–322

8 Zhang H F, Goldstein S L, Zhou X H, et al. Evolution of subcontinental lithospheric mantle beneath eastern China: Re-Os isotopic evidence from mantle xenoliths in Paleozoic kimberlites and Mesozoic basalts. Contrib Mineral Petrol, 2008, 155: 271–293

9 Yan J, Chen, J F Xie Z. Mantle derived xenoliths in the late Cretaceous basalts in eastern Shandong: New constraints on the timing of lithospheric thinning in east China. Chin Sci Bull, 2003, 48: 1570–1574

10 Ying J F, Zhang H F, Kita N, et al. Nature and evolution of Late Cretaceous lithospheric mantle beneath the eastern North China Craton: Constraints from petrology and geochemistry of peridotitic xenoliths from Junan, Shandong province, China. Earth Planet Sci Lett, 2006, 244: 622–638

11 Zhang J, Zhang H F, Ying J F, et al. Contribution of subducted Pacific slab to Late Cretaceous mafic magmatism in Qingdao region, China: A petrological record. Island Arc, 2008, 17: 231–241

12 Zhang J, Zhang H F, Kita N, et al. Secular evolution of the lithospheric mantle beneath the eastern North China craton: Evidence from peridotitic xenoliths from Late Cretaceous mafic rocks in the Jiaodong region, east-central China. Int Geol Rev, 2011, 53: 182–211

13 Engebretson D C, Cox A, Gordon R G. Relative motions between oceanic and continental plates in the Pacific basins. Geol Soc Am Spec, 1985, 206: 1–59

14 Faure M, Natal'in B. The geodynamic evolution of the eastern Eurasian margin in Mesozoic times. Tectonophysics, 1992, 208: 397–411

15 Guo F, Nakamura E, Fan W M, et al. Generation of Palaeocene adakitic andesites by magma mixing; Yanji Area, NE China. J Petrol, 2007, 48: 661–692

16 Zhang J J, Zheng Y F, Zhao Z F. Geochemical evidence for interaction between oceanic crust and lithospheric mantle in the origin of Cenozoic continental basalts in east-central China. Lithos, 2009, 110: 305–326

17 Wang Y, Zhao Z F, Zheng Y F, et al. Geochemical constraints on the nature of mantle source for Cenozoic continental basalts in east-central China. Lithos, 2011, 125: 940–955

18 Xu Z, Zhao Z F, Zheng Y F. Slab-mantle interaction for thinning of cratonic lithospheric mantle in North China: Geochemical evidence from Cenozoic continental basalts in central Shandong. Lithos, 2012, 146-147: 202–217

19 Chen L H, Zeng G, Jiang S Y, et al. Sources of Anfengshan basalts: Subducted lower crust in the Sulu UHP belt, China. Earth Planet Sci Lett, 2009, 286: 426–435

20 Dai L Q, Zhao Z F, Zheng Y F, et al. Zircon Hf-O isotope evidence for crust-mantle interaction during continental deep subduction. Earth Planet Sci Lett, 2011, 308: 229–244

21 Eiler J M. Oxygen isotope variations in basaltic lavas and upper mantle rocks. Rev Mineral Geochem, 2001, 43: 319–364

22 Valley J W. Oxygen isotopes in zircon. Rev Mineral Geochem, 2003, 53: 343–385

23 Bindeman I. Oxygen isotopes in mantle and crustal magmas as revealed by single crystal analysis. In: Putirka K D, Tepley III F J, eds. Minerals, Inclusions and Volcanic Processes. Rev Mineral Geochem, 2008, 69: 445–478

24 Zheng Y F. Metamorphic chemical geodynamics in continental subduction zones. Chem Geol, 2012, 328: 5–48

25 Li S G, Jagoutz E, Lo C H, et al. Sm/Nd, Rb/Sr, and $^{40}Ar/^{39}Ar$ isotopic systematics of the ultrahigh-pressure metamorphic rocks in the Dabie–Sulu belt, Central China: A retrospective view. Int Geol Rev, 1999, 41: 1114–1124

26 Zheng Y F, Zhou J B, Wu Y B, et al. Low-grade metamorphic rocks in the Dabie-Sulu orogenic belt: A passive-margin accretionary wedge deformed during continent subduction. Int Geol Rev, 2005, 47: 851–871

27 Fan W M, Guo F, Wang Y J, et al. Postorogenic bimodal volcanism along the Sulu orogenic belt in eastern China. Phys Chem Earth (A), 2001, 27: 733–746

28 Guo F, Fan W M, Wang Y J, et al. Origin of early Cretaceous calc-alkaline lamprophyres from the Sulu orogen in eastern China: Implications for enrichment processes beneath continental collisional belt. Lithos, 2004, 78: 291–305

29 Yang J H, Zhou X H. Rb-Sr, Sm-Nd, and Pb isotope systematics of pyrite: Implications for the age and genesis of lode gold deposits. Geology, 2001, 29: 711–714

30 Sobolev A V, Hofmann A W, Kuzmin D V, et al. The amount of recycled crust in sources of mantle-derived melts. Science, 2007, 316: 412–417

31 Li X H, Li W X, Li Q L, et al. Petrogenesis and tectonic significance of the 850 Ma Gangbian alkaline complex in South China: Evidence from *in situ* zircon U-Pb dating, Hf-O isotopes and whole-rock geochemistry. Lithos, 2010, 114: 1–15

32 Bindeman I N, Gurenko A A, Sigmarsson O, et al. Oxygen isotope heterogeneity and disequilibria of olivine phenocrysts in large volume basalts from Iceland: Evidence for magmatic digestion and erosion of Pleistocene hyaloclastites. Geochim Cosmochim Acta, 2008, 72: 4397–4420

33 Thompson R N, Gibson S A. Transient high temperatures in mantle plume heads inferred from magnesian olivines in Phanerozoic picrites. Nature, 2000, 407: 502–506

34 Chazot G, Lowry D, Menzies M, et al. Oxygen isotopic composition of hydrous and anhydrous mantle peridotites. Geochim Cosmochim Acta, 1997, 61: 161–169

35 Zhang R Y, Rumble D, Liou J G, et al. Low $\delta^{18}O$, ultrahigh-P garnet-bearing mafic and ultramafic rocks from Dabie Shan, China. Chem Geol, 1998, 150: 161–170

36 Zheng Y F, Yang J J, Gong B, et al. Partial equilibrium of radiogenic and stable isotope systems in garnet peridotite during UHP metamorphism. Am Mineral, 2003, 88: 1633–1643

37 Xu W L, Zhou Q J, Pei F P, et al. Destruction of the North China Craton: Delamination or thermal/chemical erosion? Mineral chemistry and oxygen isotope insights from websterite xenoliths. Gondwana Research, 2012, doi: 101016/jgr201202008

38 Bindeman I N, Watts K E, Schmitt A K, et al. Voluminous low-$\delta^{18}O$ magmas in the late Miocene Heise volcanic field, Idaho: Implications for the fate of Yellowstone hotspot calderas. Geology, 2007, 35: 1019–1022

39 Zheng Y F, Wu Y B, Chen F K, et al. Zircon U-Pb and oxygen isotope evidence for a large-scale ^{18}O depletion event in igneous rocks during the Neoproterozoic. Geochim Cosmochim Acta, 2004, 68: 4145–4165

40 Gregory R T, Taylor Jr H P. An oxygen isotope profile in a section of Cretaceous oceanic crust, Samail ophiolite, Oman: Evidence for ^{18}O buffering of the oceans by deep (>5 km) seawater-hydrothermal circulation at mid-ocean ridges. J Geophys Res, 1981, 86: 2737–2755
41 Putlitz B, Matthews A, Valley J W. Oxygen and hydrogen isotope study of high pressure metagabbros and metabasalts (Cyclades, Greece): Implications for the subduction of oceanic crust. Contrib Mineral Petrol, 2000, 138: 114–126
42 Harmon R S, Hoefs J. Oxygen isotope heterogeneity of the mantle deduced from global ^{18}O systematics of basalts from different geotectonic settings. Contrib Mineral Petrol, 1995, 120: 95–114
43 Eiler J M, Farley K A, Valley J W, et al. Oxygen isotope variations in oceanic island basalt phenocrysts. Geochim Cosmochim Acta, 1997, 61: 2281–2293
44 Gurenko A A, Bindeman I N, Chaussidon M. Oxygen isotope heterogeneity of the mantle beneath the Canary Islands: Insights from olivine phenocrysts. Contrib Mineral Petrol, 2011, 162: 349–363
45 Garcia M O, Ito E, Eiler J M. Oxygen isotope evidence for chemical interaction of Kilauea historical magmas with basement rocks. J Petrol, 2008 49: 757–769
46 Wang Z, Eiler J M. Insights into the origin of low-$\delta^{18}O$ basaltic magmas in Hawaii revealed from *in situ* measurements of oxygen isotope compositions of olivines. Earth Planet Sci Lett, 2008, 269: 376–386
47 Auer S, Bindeman I, Wallace P, et al. The origin of hydrous, high-$\delta^{18}O$ voluminous volcanism: Diverse oxygen isotope values and high magmatic water contents within the volcanic record of Klyuchevskoy volcano, Kamchatka, Russia. Contrib Mineral Petrol, 2008, 157: 209–230
48 Zhang H F, Ying J F, Shimoda G, et al. Importance of melt circulation and crust-mantle interaction in the lithospheric evolution beneath the North China Craton: Evidence from Mesozoic basalt-borne clinopyroxene xenocrysts and pyroxenite xenoliths. Lithos, 2007, 96: 67–89
49 Yu S Y, Xu Y G, Ma J L, et al. Remnants of oceanic lower crust in the subcontinental lithospheric mantle: Trace element and Sr-Nd-O isotope evidence from aluminous garnet pyroxenite xenoliths from Jiaohe, Northeast China. Earth Planet Sci Lett, 2010, 297: 413–422